ON THE APPLICATION TO ROBOTICS OF THE EULER-BERNOULLI BEAMS WITH EXTERNAL PATCHES

NICOLETA STAN , MARIUS IONESCU, LIGIA MUNTEANU, VALERICA MOSNEGUTU, VETURIA CHIROIU

Abstract. The paper discusses the behavior of a Euler-Bernoulli beam with external patches made from GeSbTe chalcogenide material. The nonlocal theory is used to model the damping force as a weighted average of the velocity field over a suitable distance. The resonance is avoided through a careful choosing of the patch location and the eigenvalues. The atomic-level knowledge of the material gives the route for understanding their properties necessary to specific devices.

Key words: Beam with external patches, nonlocal theory, optimization, damping.

1. CHALCOGENIDE MATERIALS

Chalcogenide materials (glasses) contain the sulphur, selenium, tellurium and the oxigen as principal constituents. The difference between the chalcogenide materials and the oxides consists in their bandgap energy which is between 1eV and 3eV [1]. These materials are not stable because the activation energy is low. In a stable state, the crystalline GeSbTe has two configurations: hexagonal and a metastable face-centered cubic (FCC) lattice. Chalcogenide materials GeSbTe have a distorted rocksalt structure with many vacancy defects and a glass transition temperature of around 100°C [1]. GeSbTe has two stable states, crystalline and amorphous. The phase change mechanism from high resistance amorphous phase to low resistance crystalline phase in nano-timescale is the most important characteristic of GeSbTe.

Because Te has an extra lone pair of electrons, the Urbach energy presents a tail in its band structure. Chalcogenide glasses display interest properties such as the photodarkening, photodissolution of metals, photoinduced anisotropy, photocrystallisation [1], photobleaching [2], photopolymerization and strong self-phase modulation [3] and photocompaction [4]. Chalcogenide materials transmit long wavelengths in the IR to around 10, 15 and 20 μm, that make them very important to the thermal imaging, night vision, CO and CO2 laser power delivery, radiometry and remote chemical analysis [5]. Their long wavelength transparency allows them to have important applications such as the chemical sensing (because

Institute of Solid Mechanics of the Romanian Academy

Ro. J. Techn. Sci. – Appl. Mechanics, Vol. 68, N° 1, P. 45–58, Bucharest, 2023

the chalcogenides vibrate in the IR region), the detecting of the contaminants in soil and various human tissues [6] (the low phonon energy of chalcogenide4swhich are due to the interaction between the large mass of their constituent atoms and the relatively weak bonds between them). We note that the chalcogenide glasses are suitable for ultra-fast switching in various telecommunication systems due to the refractive index around two orders of magnitude higher than silica.

In this paper, the damping is studied for a Euler-Bernoulli beam with external patches made from crystalline GeSbTe chalcogenide. The chalcogenide alloy GeSbTe is chosen since this material can be switched electrically in a reversible way from the crystalline to the amorphous phase. In addition, the theory of damping can be applied especially to robotics because the robot's vibrational behavior is a growing field with relatively low operating costs, compared to other disciplines.

2. THEORY OF DAMPING

The Euler-Bernoulli motion equation is expressed as [1, 7]

$$\rho(x)\frac{\partial^2}{\partial t^2}w(x,t)+M\frac{\partial}{\partial t}w(x,t)=0,\ x\in[0,L],\ t\in[0,T], \tag{1}$$

where x is the spatial variable, t is time, L is the length of the beam, and the kernel $C(x,\xi,t-\tau)$ is defibned as [7]

$$M\frac{\partial}{\partial t}w(x,t)=\int_{\Omega}\int_{0}^{t}C(x,\xi,t-\tau)\frac{\partial}{\partial t}w(\xi,\tau)\mathrm{d}\tau\mathrm{d}\xi. \tag{2}$$

Equation (1) is subjected to the initial conditions

$$w(x,0)=w_0(x),\ \frac{\partial}{\partial t}w(x,t)\,|_{t=0}=v_0(x). \tag{3}$$

We can add appropriate boundary conditions.

In the following, we consider that the kernel function can be written in the general form of a viscoelastic damping model, in which the Heaviside function denotes the presence of the damping [1, 7]

$$C(x,\xi,t-\tau)=H(x)c(x-\xi)g(t-\tau). \tag{4}$$

We have $H(x)=H_0$ (constant) if x is within the patch, and $H(x)=0$ otherwise. The term nonlocal refers to the fact that the damping of the beam depends on all points in the beam. In such cases, $C(x,\xi,t-\tau)$ depends on

$$g(t-\tau)=\delta(t-\tau), \tag{5}$$

and

$$C(x,\xi,t-\tau)=H(x)c(x-\xi)\delta(t-\tau),\ \int_{-\infty}^{\infty} c(x)\mathrm{d}x=1. \tag{6}$$

We see that from (6) that the velocities at different locations of the beam can change the value of the damping force at a given point [8–10]. The variation of the energy loss per unit volume with respect to the number of compressive cyclic loadings is considered. We see that this variation is the closest to the experimental data [11, 12].

The Poisson's ratio versus compressive strain for chalcogenide beam is presented in Fig. 1, [13]. It is interesting to see that the chalcogenide films exhibit a negative Poisson's ratio of -0.183 at compressive strain from 10 to 25%, showing a sharp increase for rising compressive strain, reaching then the zero value at 55% of compressive strain and a positive Poisson's ratio of 0.081 at 70%.

For any given loading cycle, the dissipated energy is $\int_{\varepsilon_{\min}}^{\varepsilon_{\max}} \sigma\,\mathrm{d}\varepsilon$, with $\varepsilon_{\min}$ and $\varepsilon_{\max}$ the minimum and maximum strains, respectively, and $\sigma = E\dfrac{\partial w}{\partial x}$.

Four spatial kernels are chosen to study the damping properties: the exponential decay function $\dfrac{\alpha}{2}\exp(-\beta|x-\xi|)$, the error function $\dfrac{\alpha}{\sqrt{2\pi}}\exp\left(-\dfrac{1}{2}\beta^2(x-\xi)^2\right)$, the hat function $\dfrac{1}{l_0}$ for $|x-\xi|\le\dfrac{l_0}{2}$, and 0 otherwise, and the triangular function $\dfrac{1}{l_0}\left(1-\dfrac{|x-\xi|}{l_0}\right)$ for $|x-\xi|\le l_0$, and 0 otherwise, respectively.

In all these representations, α and β are characteristic constants of the damping material and l_0 is the influence distance parameter. The numerical results are quite satisfying.

The following conclusions can be drawn from this analysis:

(1) all functions show a good correlation of the energy loss per unit volume with experimental data;
(2) the hat and triangular functions yield to similar values of energy loss per unit volume (~ 20 mJ/cm^3) after 20000 cycles,
(3) the error function and the exponential decay function are closer to an average value of 25 mJ/cm^3, and respectively, 27mJ/cm^3.

One feature of all results is the high energy dissipated by the chalcogenide patches compared to other materials for the same loading level.

Therefore, we choose for the spatial kernel function the exponential decay with $\beta = \alpha \frac{1+\nu}{E}$ and $\alpha = 0.22$

$$c(x-\xi) = \frac{\alpha}{2} \exp\left(-\alpha \frac{1+\nu}{E} | x-\xi | \right). \tag{7}$$

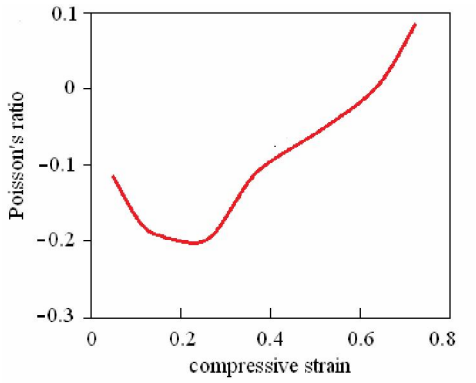

Fig. 1 – Poisson's ratio versus compressive strain for chalcogenide beam (from [13]).

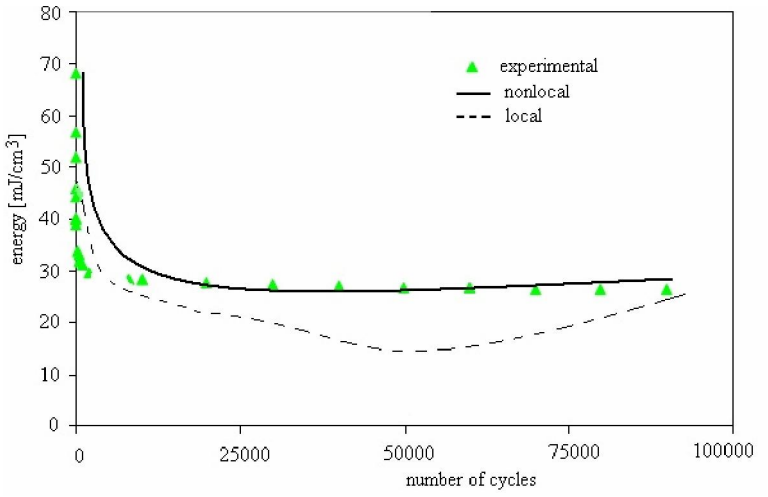

Fig. 2 – Damping capacity of the beam with an external chalcogenide path (local, nonlocal and experimental).

In Fig. 2 we present the energy loss per unit volume (mJ/cm) versus the number of compressive cyclic loading for the beam, obtained by the local theory, nonlocal theory with spatial kernel function given by (7) and experiments [1,11,12]. A minimum value around 50000 cycles is observed denoting the energy increase. While the nonlocal and experimental values of the energy have similar values after 20000 cycles, the local values are lower with a decrease by 35.5%.

3. EQUATION OF MOTION

The external patches are attached at $(x_1, x_1 + \Delta x_1)$, $(x_2, x_2 + \Delta x_2)$..... $(x_k, x_k + \Delta x_k)$, $x_2 \geq x_1 + \Delta x_1$, $x_i \geq x_{i-1} + \Delta x_{i-1}$, $i = 2,...,k$, as shown in Fig. 3 [14]. The parameters x_j and Δx_j, $j = 1,2,...,k_p$, are subjected to the conditions $x_2 \geq x_1 + \Delta x_1$, $x_i \geq x_{i-1} + \Delta x_{i-1}$, $i = 2,...,k_p$. The equation of motion is given by [1]

$$\frac{\partial}{\partial x^2}\left(EI(x)\frac{\partial^2 w(x,t)}{\partial x^2} \right) + \rho A(x)\frac{\partial^2 w(x,t)}{\partial t^2} + \Upsilon(x,t) = 0. \tag{8}$$

The term $\Upsilon(x,t)$ is a nonlocal function that expresses the external damping defined over $(x_i, x_i + \Delta x_i)$, $i = 1,2,...,k$, ([14], [20]) as

$$\Upsilon(x,t) = \int_{x_i}^{x_i+\Delta x_i} \int_{-\infty}^{t} C(x,\xi,t-\tau)\frac{\partial w(\xi,\tau)}{\partial t} \mathrm{d}\tau \mathrm{d}\xi . \tag{9}$$

The damping kernel $C(x,\xi,t-\tau)$ is defined by (7) and (9). We write the initial conditions (3) under the form

$$w(x,0) = w_0(x), \ \frac{\partial}{\partial t} w(x,t)|_{t=0} = v_0(x). \tag{10}$$

For a cantilever beam, the boundary conditions are

$$\begin{aligned} &w(x,t) = 0, \frac{\partial w(x,t)}{\partial x} = 0 \text{ for } x = 0, \\ &\frac{\partial^2 w(x,t)}{\partial x^2} = 0, \ \frac{\partial^3 w(x,t)}{\partial x^3} = 0 \ \text{ for } x = L. \end{aligned} \tag{11}$$

The eigenfrequency problem (8)–(11) can be analytically solved by using the cnoidal method [15, 16].

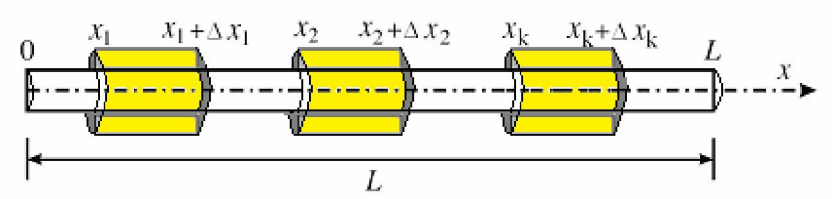

Fig. 3 – The beam with external chalcogenide patches.

The solutions of (8) can be write generally as a sum of Jacobian elliptic functions (cnoidal functions) [1]

$$w(x,t)=\sum_{j=1}^{N} A_j \mathrm{cn}^2(\eta \mid m_j),\ \eta = kx-\omega t+\varphi, \tag{12}$$

with N the number of functions, A_j are unknown constants, k is the wave number, ω is the frequency and φ is the phase. Writing $\eta \mid m_j = \eta_j$ and substituting (12) into (8) we have

$$\frac{\partial}{\partial x^2}\left(EI(x)\frac{\partial^2}{\partial x^2}\left(\sum_{j=1}^{N} A_j \mathrm{cn}^2\eta_j\right)\right)+\rho A(x)\frac{\partial^2}{\partial t^2}\left(\sum_{j=1}^{N} A_j \mathrm{cn}^2\eta_j\right)+\Upsilon=0, \tag{13}$$

with

$$\Upsilon=\int_{x_i}^{x_i+\Delta x_i}\int_{-\infty}^{t} C(x,\xi,t-\tau)\frac{\partial}{\partial t}\left(\sum_{j=1}^{N} A_j \mathrm{cn}^2\zeta_j\right)\mathrm{d}\tau\mathrm{d}\xi, \tag{14}$$
$$\zeta_j = k_j\xi-\omega_j\tau+\varphi_j.$$

By solving the eigenvalue problem (13) and (14), the eigenvalues are found along with the associated conditions (10).

4. THE FORWARD PROBLEM

Equations (13) and (14) are reduced to the eigenvalue equation

$$\sum_{j=1}^{N}(P_j+\rho\omega^2 Q_j+\omega R_j+\Upsilon_j)=0, \tag{15}$$

where P,Q,R are polynomials in functions cn, sn and dn. The functions Υ_j,

$i = 1, 2, ..., N$, are

$$\Upsilon_j = 2\omega A_j \sum_{i=1}^{k} \int_{x_i}^{x_i+\Delta x_i} \int_{-\infty}^{t} C(x, \xi, t-\tau)(\mathrm{cn}\eta_j \mathrm{sn}\eta_j \mathrm{dn}\eta_j)\mathrm{d}\tau\mathrm{d}\xi,$$
$$\eta_j = \eta \,|\, m_j = k\xi - \omega\tau + \varphi. \tag{16}$$

The equation (15) is solved by using the cnoidal method and equating the terms with the same power in the functions cn, sn and dn. From (15) we have K equations $\lambda_1(A_j, m_j, k, \varphi) = \omega_1$,

$$\lambda_2(A_j, m_j, k, \varphi) = \omega_2, \quad \lambda_K(A_j, m_j, k, \varphi) = \omega_K. \tag{17}$$

The number of unknowns of the problem are $p_M = \{A_j, m_j, k, \varphi, \omega, j = 1, 2..., k\}$, $M = 2k + 3$. Because, the number of unknowns is greater than the number of equations $K < M$, we introduce a restrictive approach for solving (15) by using the residual functions r_K expressed as

$$\lambda_l(A_j, m_j, k, \varphi) - \omega_l = r_l, \; l = 1, 2, ..., K. \tag{18}$$

The minimization problem is solved by combining the residuals in order to compute the p_M. The eigenfrequency problem is solved by a least-squares algorithm with the objective function

$$\Im(p_j) = K^{-1} \sum_{l=1}^{K} r_l{}^2(p_j) + (4N_1)^{-1} \sum_{n=1}^{N_1} \sum_{i=1}^{2} \delta_{i\mathrm{n}}^2(p_j) + \sum_{j=1}^{6} \delta_j^2(p_j), \tag{19}$$

with $\delta_{in}(p_j)$, $i = 1, 2$, $n = 1, 2, ..., N_1$, the control indicators that verify the satisfaction of the initial conditions (10) at x_n, $n = 1, 2, ..., N_1$

$$\delta_{1n} = w(x_n, 0) - w_0(x_n), \; \delta_{2n} = \frac{\partial}{\partial t} w(x_n, 0) - v_0(x_n). \tag{20}$$

The boundary conditions (11) introduce six control indicators to verify the conditions for a clamped beam

$$\delta_3 = w(0,0), \; \delta_4 = w(L,0), \; \delta_5 = \frac{\partial w(0,0)}{\partial x}, \; \delta_6 = \frac{\partial w(L,0)}{\partial x}, \tag{21}$$

for a simply supported beam

$$\delta_3 = w(0,0), \delta_4 = w(L,0), \delta_5 = \frac{\partial^2 w(0,0)}{\partial x^2}, \delta_6 = \frac{\partial^2 w(L,0)}{\partial x^2}, \tag{22}$$

or a free end beam

$$\delta_3 = \frac{\partial^2 w(0,0)}{\partial x^2}, \delta_4 = \frac{\partial^2 w(L,0)}{\partial x^2}, \delta_5 = \frac{\partial}{\partial x}\left[EI(0)\frac{\partial^2 w(0,0)}{\partial x^2} \right]. \tag{23}$$

The unknowns $p_M = \{A_j, m_j, k, \varphi, \omega, j = 1,2...,k\}$, $M = 2k+3$, are determined by using a genetic algorithm.

5. THE INVERSE APPROACH

In the formulation of the inverse problem, the bound optimization formulation presented in [32–35] is used. The unknown parameters are the positions of the patches x_j and their lengths Δx_j, $j = 1,2,...,k_p$, under the conditions $x_2 \geq x_1 + \Delta x_1$, $x_i \geq x_{i-1} + \Delta x_{i-1}$, $i = 2,...,k_p$.

The inverse problem consists of determining x_j, Δx_j, $j = 1,2,...,k_p$, so that (16) and (17) are satisfied, and all eigenvalues to stay above a given complex constant $C_1 + \mathrm{i}C_2$. The formulation of the optimization problem is:

$$\begin{gathered}
\text{Find } x_j,\ \Delta x_j,\ j = 1,2,...,k_p, \text{ from the maximization approach [1]} \\
\text{maximize } |C_1|,\ |C_2| \\
\text{subject to : all } \mathrm{Re}\,|\omega| \geq |C_1|,\ \mathrm{Im}\,|\omega| \geq |C_2| \\
\sum_{j=1}^{N} (P_j + \rho\omega^2 Q_j + \omega R_j + \Upsilon_j) = 0, \\
\Upsilon_j = 2\omega A_j \sum_{i=1}^{k} \int_{x_i}^{x_i+\Delta x_i} \int_{-\infty}^{t} C(x,\xi,t-\tau)(\mathrm{cn}\eta_j \mathrm{sn}\eta_j \mathrm{dn}\eta_j)\mathrm{d}\tau\mathrm{d}\xi, \\
\eta_j = \eta\,|\,m_j = k\xi - \omega\tau + \varphi,
\end{gathered} \tag{24}$$

with P, Q, R are polynomials in cn, sn and dn.

Another approach is to maximize the difference between two consecutive eigenvalues, say ω_i and ω_{i+1}, the problem can be formulated as:

$$\begin{gathered}
\text{Find } x_j,\ \Delta x_j,\ j = 1,2,...,k_p, \text{ from the maximization approach:} \\
\text{maximize } \mathrm{Re}\,|C_3 - C_4|,\ \mathrm{Im}\,|C_3 - C_4| \\
\text{subject to : } \mathrm{Re}\,|\omega_i| \geq \mathrm{Re}\,|C_4|,\ \mathrm{Re}\,|\omega_{i+1}| \geq \mathrm{Re}\,|C_3|, \\
\mathrm{Im}\,|\omega_i| \geq \mathrm{Im}\,|C_3|,\ \mathrm{Im}\,|\omega_{i+1}| \geq \mathrm{Im}\,|C_4| \\
\sum_{j=1}^{N} (P_j + \rho\omega^2 Q_j + \omega R_j + \Upsilon_j) = 0,
\end{gathered} \tag{25}$$

$$\Upsilon_j = 2\omega A_j \sum_{i=1}^{k} \int_{x_i}^{x_i+\Delta x_i} \int_{-\infty}^{t} C(x,\xi,t-\tau)(\mathrm{cn}\eta_j \mathrm{sn}\eta_j \mathrm{dn}\eta_j)\mathrm{d}\tau\mathrm{d}\xi.,$$

$$\eta_j = \eta \,|\, m_j = k\xi - \omega\tau + \varphi\,.$$

We can manipulate the eigenvalues of a structure by varying the positions of the patches within given limits dictated by the specific demands of each problem.

6. APPLICATIONS

Let us apply the theory to a cantilever beam with a patch made of the chalcogenide material GeSbTe. The properties of the beam are reported in [20] with $\alpha = 5$.

In the case of a chalcogenide patch, the negative Poisson's ratio is $\nu = -0.35$ and $\alpha = 0.22$.

In [20], the approximate solutions for the complex eigenvalues and modes with nonlocal damping are obtained by using the Galerkin method. Our numerical results are similar to those obtained by applying the Galerkin method [20]. The effect of the chalcogenide patch on the mode shapes isa discussed next. Fig. 4 shows the real and imaginary parts of the first four mode shapes for a cantilever beam with the chalcogenide material (the solid line) and viscous patches (dashed line), respectively. In the case of the chalcogenide patch, we see that the mode shapes are different from those corresponding to the traditional viscous patch.

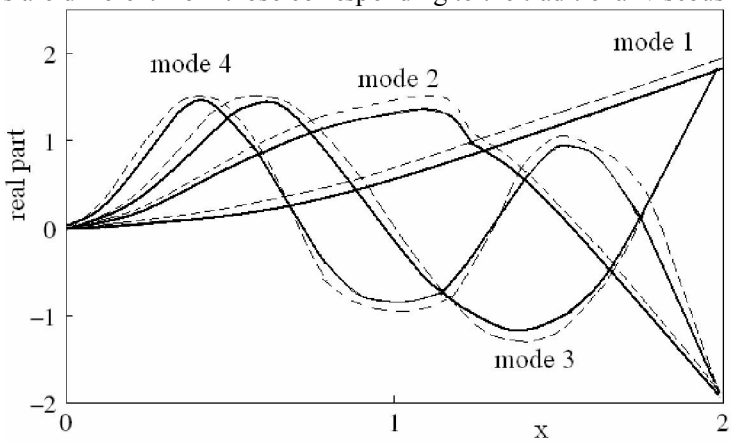

Fig. 4 – Real parts of the first four mode shapes of a cantilever beam with chalcogenide patch (solid line) and viscous patch (dashed line).

We restrict our attention on a cantilever aluminum beam of $L = 2\mathrm{m}$, of circular cross section diameter $d = 0.005\mathrm{m}$, Young's modulus $E = 70\mathrm{GPa}$, $\rho = 2700\,\mathrm{kg/m^3}$, Poisson's ratio $\nu = 0.35$, with $k_p = 0,1,2$ and 3, and $\alpha = 0.22$. The chalcogenide material has a negative Poisson's ratio, $\nu = -0.32$. The number N

of cnoidal functions is 4. For $N > 4$ the increase in the accuracy of the results obtained using the genetic algorithm is not significant.

Firstly, we compare the frequency responses of the beam with 0, 1, 2 and 3 patches (symmetrically located with respect to the beam ends). Fig. 5 displays the frequency response of the beam for 0 and 1 patch, respectively, and Fig. 6 for 2 and 3 patches, respectively. It can be seen from these figures that the amplitude of the vibration is diminished as the number of patches increases.

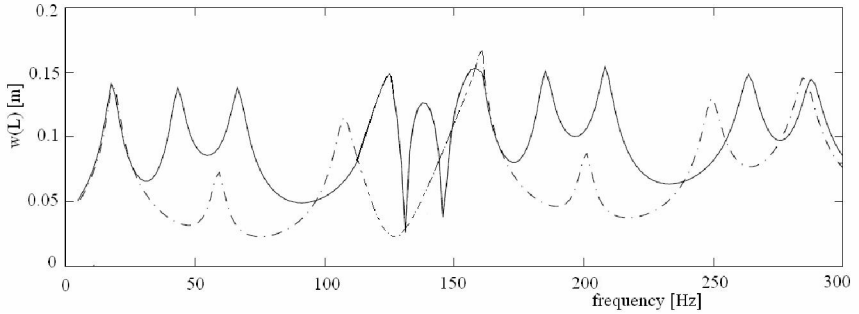

Fig. 5 – Frequency response for 0 (solid line) and 1 auxetic (dashed line) patches.

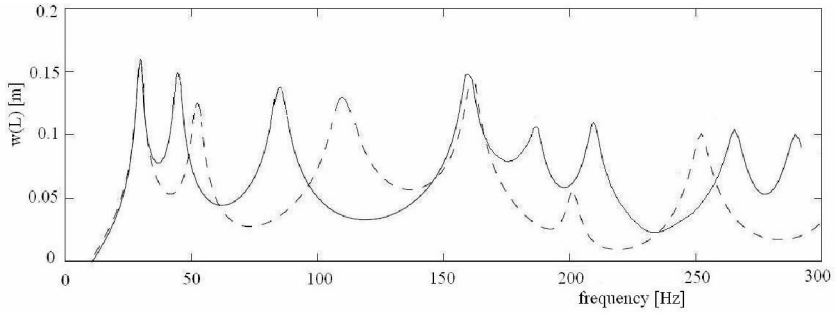

Fig. 6 – Frequency response for 2 (solid line), and 3 (dashed line) auxetic patches.

So far, we have considered the forward problem, where the number and location of the patches are known. Recall that the inverse problem determines the location of the patches by maximizing the eigenvalues or the gap between them in order to avoid resonance. Table 1 shows the five eigenfrequencies for non-optimized cantilever beam with 0, 1,2 and 3 auxetic patches, located symmetrically with respect to the ends of the beam.

Table 1

The first five eigenvalues for a cantilever beam with chalcogenide patches.

Number patches	Mode 1	Mode 2	Mode 3	Mode 4	Mode 5
0	-2.17 ± 12.51i	-1.48 ± 60.62	-1.31 ± 136.59i	-0.72 ± 280.71i	-0.052 ± 445.60i
1	-4.74 ± 19.34i	-0.30 ± 7.56i	-0.351 ± 151.53i	-0.031 ± 229.76i	-0.0031 ± 457.71i
2	-5.07 ± 20.87i	-1.11 ± 72.72i	-0.129 ± 130.49i	-0.076 ± 297.91i	-0.0173 ± 448.52i
3	-4.39 ± 17.75i	-1.79 ± 70.78i	-0.196 ± 130.63i	-.0432 ± 280.56i	-0.079 ± 445.34i

The inverse problem is solved for 3 chalcogenide patches (symmetrically located with respect to the beam ends). The unknowns are x_1, x_2, x_3, $\Delta x_1, \Delta x_2, \Delta x_3$, while the known quantity is $h_p = 0.003$m. The inverse problem (23) is solved for $C_1 + \mathrm{i}C_2 = -0.005 + 681.4\mathrm{i}$, and the problem (24) and (25) for $C_3 = -0.0066 + 681.43\mathrm{i}$, and $C_4 = -0.0025 + 233.13\mathrm{i}$.

Tables 2 and 3 present the estimates of (23) and respectively (24, 25), we mean the location and dimensions of the patches and the first six eigenvalues of the beam. Due to the symmetry of the problem, the results are reported only for x_1, Δx_1 and Δx_2 since all simulations give $x_2 = 1$ and the patch x_3 is symmetric with x_1, with respect to the middle of the beam, and $\Delta x_1 = \Delta x_3$. It can be seen from these tables that all eigenvalues stay above the complex constant $C_1 + \mathrm{i}C_2$ for (23) and the difference between two consecutive eigenvalues are maximized for (24), respectively. It is observed that x_1 is moving towards the middle of the beam when the mode increases, and the length of the patches decreases for superior modes. The optimization problem (24) gives lower values for all estimates in comparison with problem (23).

Table 2

Problem (23): Location and dimensions of the patches and the first six eigenvalues.

	Mode 1	Mode 2	Mode 3
	-4.39 ± 17.75i	-1.79 ± 70.58i	-0.196 ± 130.63i
x_1	0.034	0.040	0.058
Δx_1	0.190	0.180	0.176
Δx_2	0.175	0.167	0.168
	Mode 4	Mode 5	Mode 6
	-.0432 ± 280.56i	-0.079 ± 445.34i	-0.84 ± 3455.25i
x_1	0.056	0.072	0.070
Δx_1	0.166	0.176	0.183
Δx_2	0.155	0.141	0.144

Table 3

Problem (24): Location and dimensions of the patches and the first six eigenvalues.

	Mode 1	Mode 2	Mode 3
	-4.39 ± 17.75i	-1.79 ± 70.58i	-0.196 ± 130.63i
x_1	0.056	0.044	0.047
Δx_1	0.179	0.158	0.141
Δx_2	0.164	0.133	0.139
	Mode 4	Mode 5	Mode 6
	-0.432 ± 280.56i	-0.079 ± 445,34i	-0.84 ± 3455.25i
x_1	0.057	0.061	0.077
Δx_1	0.132	0.145	0.122
Δx_2	0.133	0.118	0.113

7. CONCLUSIONS

The paper describes a model of a beam with chalcogenide patches. The damping force is considered as a weighted average of the velocity over the spatial field. The kernel function is based on the distance measures. The spatial kernel function is constructed on the experimentally data of the energy loss per unit volume with respect to the number of compressive loadings.

The design optimization of the beam with chalcogenide external patches avoid resonance through a carefully choose of the location of the patches through the maximization of the eigenfrequencies of the beam or the gap between them. The examples show that we can improve the damping capacity of the beam by choosing the external patches at the same time being possible to avoid resonance by manipulating the eigenfrequencies.

The study of beams with chalcogenide patches promises to make more understandable the damping properties of the beams that use the chalcogenide material to add damping to them. On the other hand, it provides the fundaments for the fabrication of new composites with tailored properties and improved damping properties, opening the door to new applications. Materials with chalcogenide patches easily undergo volume changes and resist shape changes and may thus be viewed as the opposite of silicon and oxides.

Acknowledgements. The financial support received by Romanian Ministry of Research and Innovation PNCDI III project PN-III-P2-2.1-PED-2019-0085 CONTRACT 447PED/2020 is gratefully acknowledged. The authors also thank the referees for their useful comments.

Received on November 15, 2022

REFERENCES

1. CHIROIU, V., MUNTEANU, L., DONESCU, S., *On the beams with external auxetic patches*, Advances in Mechanical Engineerings, **1**, SAGE Journals, 2009, 10.1155/2009/430379.
2. LAKES, R. S., *Experimental Microelasticity of Two Porous Solids*, Int. J. Solids, Structures, **22**, *1*, pp. 55–63, 1986.
3. LAKES, R. S., *Foam structures with a negative Poisson's ratio*, Science, **235**, *4792*, pp. 1038–1040, 1987.
4. LAKES, R. S., *Experimental micro mechanics methods for conventional and negative Poisson's ratio cellular solids as Cosserat continua*, J. Engineering Materials and Technology, **113**, *1*, pp. 148–155, 1991.
5. OVERAKER, D.W., CUITIÑO, L.M., LANGRANA, N.A., *Effects of morphology and orientation on the behavior of two-dimensional hexagonal foams and application in a re-entrant foam anchor model*, Mech. Mater., **29**, *1*, pp. 43–52,1998.
6. WANG, Y.-C., LAKES, R., *Analytical parametric analysis of the contact problem of human buttocks and negative Poisson's ratio foam cushions*, Int. J. Solids Structures, 39, *18*, pp. 4825–4838, 2002.
7. LOVE, A. E. H., *A treatise on the mathematical theory of elasticity*, 4th ed., Dover, New York, 1926.
8. GUNTON, D.J., SAUNDERS, G.A., *Stability Limits on the Poisson Ratio*, *J. Mater. Sci.*, 7, .pp. 1061–1068, 1972.
9. LI, Y., *The anisotropic behavior of Poisson's ratio, Young's modulus, and shear modulus in hexagonal materials*, Phys. Status Solidi, **38**, *1*, pp. 171–175, 1976.
10. BAUGHMAN, R.H., SHACKLETTE, J.M., ZAKHIDOV, A.A., STAFSTROM, S., *Negative Poisson's ratios as a common feature of cubic metals*, Nature, 392, pp. 362–365, 1998.
11. SCARPA, F., GIACOMIN, J.A., BEZAZI, A., BULLOUGH, W.A., *Dynamic behaviour and damping capacity of auxetic foam pads*, SPIE Proceeding, **6169**, Smart Structures and Materials 2006: Damping and Isolation, William W. Clark, Mehdi Ahmadian, Arnold Lumsdaine, Editors, 61690T, 2006.
12. DONESCU, S., CHIROIU, V., MUNTEANU, L., *On the Young's modulus of a auxetic composite structure*, Mechanics Research Communications, **36**, *3*, pp. 294–301, 2009.
13. DONESCU, S., MUNTEANU, L., DELSANTO, P.P., MOSNEGUTU, V., Ch.4: *On the advanced auxetic composites*, Research Trends in Mechanics, **3**, Ed. Academiei, 2009.
14. CHIROIU, V., DONESCU, S., MUNTEANU, L., MOSNEGUTU, V., *The dynamics of beams with auxetic patches*, Proceedings of the International Conference on Advanced Materials for Application in Acoustics and Vibration AMAAV'09, The British University of Egypt, 4–6 January, Cairo, 2009.
15. MUNTEANU, L., DUMITRU, D., DONESCU, S., CHIROIU, V., *On the complexity of the auxetic systems*, part VIII, ch. 65, Proceedings of the European Computing Conference, Lecture Notes in Electrical Engineering 28, **2** (eds. N.Mastorakis, V.Mladenov), Springer-Verlag, pp. 631–636, 2009.
16. SCARPA, F., PASTORINO, P., GARELLI, A., PATSIAS, S., RUZZENE, M., *Auxetic Compliant Flexible PU Foams: Static and Dynamic Properties*, Physica Status Solidi B, **242**, *3*, pp. 681–694, 2005.
17. FRISWELL, M. I, ADHIKARI, S., LEI, Y., *Non-local finite element analysis of damped beams*, International Journal of Solids and Structures, **44**, *22–23*, pp. 7564–7576, 2007.
18. FRISWELL, M. I, ADHIKARI, S., LEI, Y., *Vibration analysis of beams with non-local foundations using the finite element method*, International Journal of Numerical Methods in Engineering, **71**, *11*, pp. 1365–1386, 2007.
19. FLUGGE, W., *Viscoelasticity*, 2nd ed. Springer-Verlag, Berlin, 1975.
20. LEI, Y., FRISWELL, M.I., ADHIKARI, S., *A Galerkin method for distributed systems with nonlocal damping*, International Journal of Solids and Structures, **43**, pp. 3381–3400, 2006.

21. GHONEIM, H., *Fluid surface damping versus constrained layer damping for vibration suppression of simply supported beams*, Smart Materials and Structures, 6, pp. 40–46, 1997.
22. ADHIKARI, S., *Dynamics of non-viscously damped linear systems*, ASCE Journal of Engineering Mechanics, **128**, *3*, pp. 328–339, 2002.
23. ADHIKARI, S., LEI, Y., FRISWELL, M. I., *Modal analysis of non-viscously damped beams*, Transactions of ASME, Journal of Applied Mechanics, **74**, *5*, pp. 1026–1030, 2007.
24. WAGNER, N., ADHIKARI, S., *Symmetric state-space formulation for a class of non-viscously damped systems*, AIAA Journal, **41**, *5*,pp. 951–956, 2003.
25. BANKS, H.T., INMAN, D.J., *On damping mechanisms in beams*, Journal of Applied Mechanics, **58**, *3*, pp. 716–723, 1991.
26. BANKS, H.T., WANG, Y. INMAN, D.J., *Bending and shear damping in beams-frequency-domain estimation techniques*, Journal of Vibration and Acoustics, **116**, *2*, pp. 188–197, 1994.
27. SORRENTINO, S., MARCHESIELLO, S., PIOMBO, B.A.D., *A new analytical technique for vibration analysis of non-proportionally damped beams*, Journal of Sound and Vibration, **265**, *4*, pp. 765–782, 2003.
28. BEZAZI, A., SCARPA, F., *Mechanical behaviour of conventional and negative Poisson's ratio thermoplastic polyurethane foams under compressive cyclic loading*, International Journal of Fatigue, **29**, *5*, pp. 922–930, 2007.
29. CHIROIU, V., *On the eigenvalues optimization of beams with damping patches*, New Aspects of Engineering Mechanics Structures, Geology, Mathematics and Computers in Science Engineering, A Series of Reference Books and Textbooks, (EMESEG '09) Heraklion, WSEAS Press, pp. 117–122, 2008.
30. MUNTEANU, L., DONESCU, S., *Introduction to Soliton Theory: Applications to Mechanics, Book Series "Fundamental Theories of Physics"*, 143, Kluwer Academic Publishers, 2004.
31. CHIROIU, V., CHIROIU, C., *Probleme inverse in mecanica* (Inverse problems in mechanics), Ed. Academiei, Bucharest, 2003.
32. BENDSOE, M..P., OLHOFF, N., TAYLOR, J.E., *A variational formulation for multicriteria structural optimization*, Journal of Structural Mechanics, **11**, *4*, pp. 523–544, 1983.
33. PEDERSEN, N.L., *Designing plates for minimum internal resonance*, Struct. Multidisc. Optim., **28**, *1*, pp. 1–10, 2004.
34. PEDERSEN, N.L., *Optimization of holes in plates for control of eigenfrequencies*, Struct. Multidisc. Optim., **30**, *4*, pp. 297–307, 2005.
35. PEDERSEN, N.L., *On simultaneous shape and orientational design for eigenfrequency optimisation*, Danish Center for Applied Mathematics and Mechanics, report nr.714, 2006.